SANDIA REPORT
SAND2008-6123
Unlimited Release
Printed September 2008

Feasibility Study of Measuring the Temperature and Pressure of Warm Dense Matter (LDRD 08-1429)

Patrick Rambo and Jens Schwarz

Prepared by
Sandia National Laboratories
Albuquerque, New Mexico 87185 and Livermore, California 94550

Sandia is a multiprogram laboratory operated by Sandia Corporation,
a Lockheed Martin Company, for the United States Department of Energy's
National Nuclear Security Administration under Contract DE-AC04-94AL85000.

Issued by Sandia National Laboratories, operated for the United States Department of Energy by Sandia Corporation.

Available to DOE and DOE contractors from
U.S. Department of Energy
Office of Scientific and Technical Information
P.O. Box 62
Oak Ridge, TN 37831

Telephone: (865) 576-8401
Facsimile: (865) 576-5728
E-Mail: reports@adonis.osti.gov
Online ordering: http://www.osti.gov/bridge

Available to the public from
U.S. Department of Commerce
National Technical Information Service
5285 Port Royal Rd.
Springfield, VA 22161

Telephone: (800) 553-6847
Facsimile: (703) 605-6900
E-Mail: orders@ntis.fedworld.gov
Online order: http://www.ntis.gov/help/ordermethods.asp?loc=7-4-0#online

SAND2008-6123
Unlimited Release
Printed September 2008

Feasibility Study of Measuring the Temperature and Pressure of Warm Dense Matter

Patrick Rambo, Jens Schwarz
Z-Backlighter Laser Facility
Sandia National Laboratories
P.O. Box 5800
Albuquerque, New Mexico 87185-MS1193

Abstract

We have investigated the feasibility of making accurate measurements of the temperature and pressure of solid-density samples rapidly heated by the Z-Petawatt laser to warm dense matter (WDM) conditions, with temperatures approaching 100eV. The study focused specifically on the heating caused by laser generated proton beams. Based on an extensive literature search and numerical investigations, a WDM experiment is proposed which will accurately measure temperature and pressure based on optical emission from the surface and sample expansion velocity.

CONTENTS

FIGURES

TABLES

NOMENCLATURE

CCD	charge coupled device
CPI	chirped pulse interferometry
dB	decibel
DOE	Department of Energy
EMI	electromagnetic interference
EOS	Equation of State
eV	electron Volts
HV	high voltage
ICF	Inertial Confinement Fusion
IP	image plate
OTR	optical transition radiation
RCF	radiochromic film
SNL	Sandia National Laboratories
SOP	streaked optical pyrometry
TNSA	Target Normal Sheath Acceleration
WDM	Warm Dense Matter

1. INTRODUCTION

Warm dense matter (WDM) describes the difficult region between plasma and condensed matter physics, relevant to astrophysics and inertial confinement fusion (ICF). WDM equations of state are difficult to model due to the interaction of condensed matter and plasma physics. WDM cannot be forcibly confined in the lab since its pressure is on the order of Mbar at temperatures <100eV. Furthermore, more traditional shock heating experiments cannot fully constrain the WDM equations of state (since data is only along hugoniots) and thus cannot fully describe WDM. The proposed research explores WDM produced through isochoric heating of solid materials to temperatures in the 1-100eV range. Isochoric heating (i.e. heating at constant volume/density) can be achieved if the heating timescale is sufficiently shorter than the material's expansion timescale ($t \sim d/c_s$ for material thickness d and sound speed c_s). This approach accesses a different range of parameters (higher temperatures at near solid density) from the more well established shock data. To create such isochoric heating conditions is a topic of much research in recent years due to the new availability of high intensity lasers which can generate such a prompt heating event.

2. LASER-BASED ISOCHORIC HEATING APPROACHES

2.1 Direct Heating in Laser Target

When focusing a high laser intensity of the order of 10^{19} W/cm^2 onto a target foil, the beam can directly heat the target to keV level temperatures[1-3]. The absorption process has a small skin depth (<10nm) which will require the use of thin or tamped targets[4]. To prevent "target burn through" due to low energy laser pre-pulses, a high temporal contrast ratio is required. Heating via direct laser illumination always has an indirect component due to Ohmic heating.

2.2 Indirect Heating in Laser Target

At intensities of the order of 10^{19} W/cm^2, the laser drives a high current through the sample which heats the target (Figure 1) through Ohmic/resistive losses[4-7]. Laser-to-electron energy conversion efficiency is ~10^{-1} and the resulting heat deposition can be up to keV at target center down to 100eV at the target edges. Electrons can reflux multiple times through the target which will enhance the heating effect, with the lateral spread of the electrons reducing this heating effect further from the laser spot. Based on that effect, target heating is reduced for wide targets and improved for smaller width targets since they can confine the lateral electron spread. The Ohmic heating and resulting x-ray production is subject to spatial inhomogeneities due to spatial gradients (filamentation) in these high currents (suprathermal electrons) which deposit energies deep in target[4]. Inhomogeneity also drives the use of thin targets (<100nm)[4]and is one of the reasons such heating may not be as favorable as other methods for a clean isochoric heating experiment.

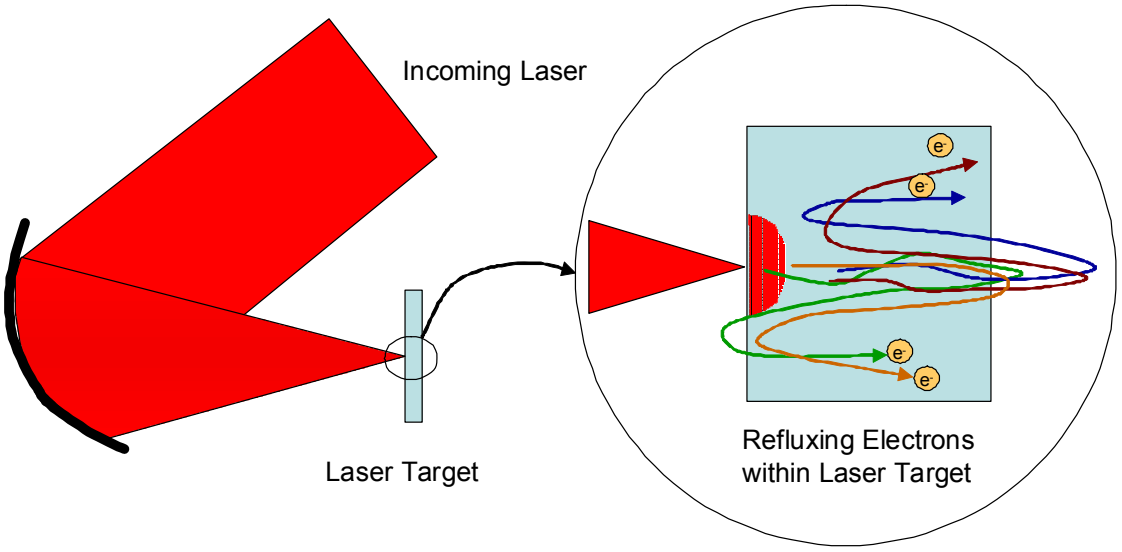

Figure 1. Ohmic heating by repeated reflux of electrons through the target

2.3 X-ray Indirect Heating

In this scenario a laser intensity of about 10^{17} W/cm^2 is used to create x-rays at an energy conversion efficiency of ~10^{-4}. X-rays from the source (which is a similar duration to laser) propagate to the secondary target (Figure 2) where they absorb throughout volume[8]. For some WDM work (specifically equation-of-state work), heating must be faster than $t \sim d/c_s$ (to be isochoric) but in turn the expansion time t must be longer than the electron-ion equilibration time (1-10ps). This requires volumetric heating of ~μm thick targets for heating pulsewidths of ~1ps and $c_s \sim 10^6$cm/s. This presents a problem for direct laser heating (due to the small skin depth) but works well for x-rays, electrons, and protons. X-rays in the 2-10keV range absorb in 2-10μm for most solids. The heating is prompt, follows direct lines-of-sight, and has well characterized absorption cross-sections. Those can be matched to a source x-ray line to increase absorption, i.e. Si k-α x-ray source to Al absorption edge.

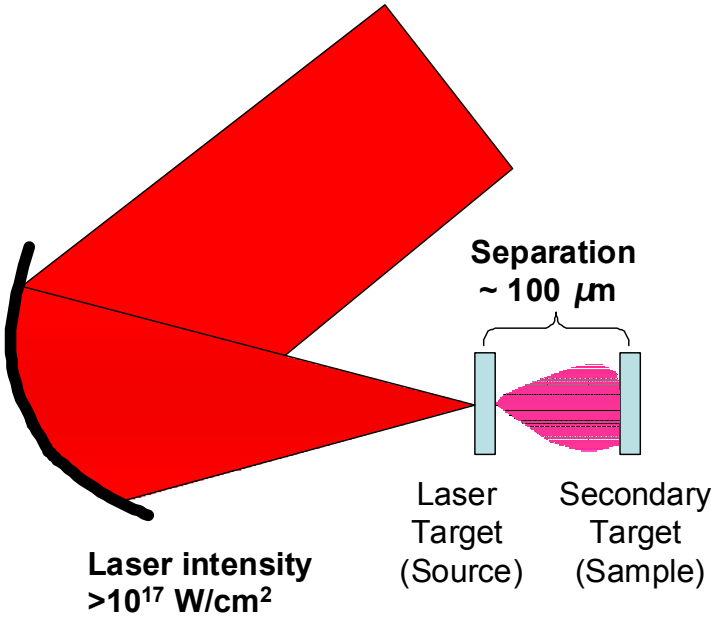

Figure 2. Indirect heating of a secondary target by x-rays created from the source target

This process is subject to subsequent heating from other accompanying effects such as protons and co-moving electrons. A source-sample separation large enough can avoid the effect of source refluxing electrons whereas lower laser intensities avoid the hot suprathermal electrons and reduce proton numbers and energies. However, these collateral effects can still overwhelm the x-ray heating, making x-ray heating less favorable than other methods.

2.4 Proton Indirect Heating

2.4.1 Generation of Proton Beam via TNSA

Laser intensities of 10^{19} W/cm^2 can be used to generate MeV scale proton beams via Target Normal Sheath acceleration[9] (TNSA) with a laser to proton energy conversion efficiency of ~10^{-2}. In this scenario, pre-plasma electrons launch through the target foil and out the rear surface where they create an electron cloud/sheath. This establishes a high electric field normal to the rear surface which field ionizes hydrocarbon contaminants on the rear surface. The electrostatic field accelerates the resulting protons which co-propagate with the electrons in a charge neutral cloud. Acceleration occurs within 0.1-10ps of the main pulse requiring a minimal sheath depth of <10μm (Debye length) at the rear surface.

In the TNSA process, lower energy protons have a large divergence angle whereas higher energy protons have a shallower divergence angle. In general, tight collimation/low emittance can be achieved due to overall charge neutrality. Finally, proton energies range from a few MeV to energies up to ~50MeV, with this distinct high energy cut-off depending on laser intensity (Figure 3).

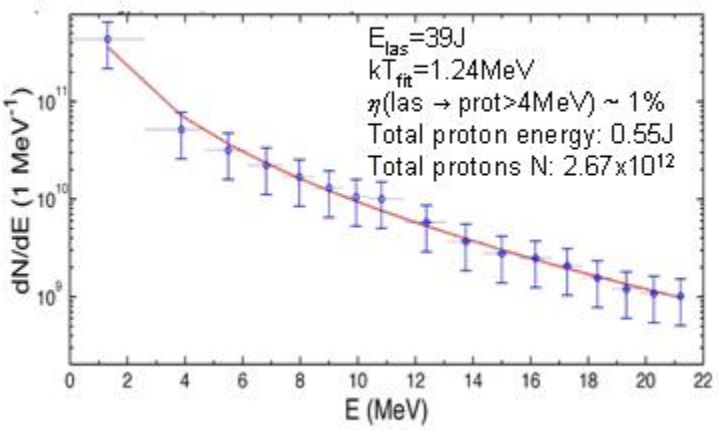

Figure 3. Number of protons vs. proton energy. Data from SNL 100TW laser.

2.4.2. Proton Target Heating

In proton isochoric heating, TNSA generated protons from the source target (lagging the prompt source x-rays) impinge onto the secondary (sample) target where they absorb throughout the volume (Figure 2) and heat the sample to the 10 eV scale[6, 10-14]. Those protons are normal to the source rear surface but can be focused with hemi-spherical foils for higher local heating. Higher Z materials show greater proton heating due to higher proton stopping power. One

should note that the sample is subject to subsequent heating from x-rays and co-moving electrons.

Foil separations are affected by several effects. First, the heated sample target should be >10μm from the source so as not to interfere with the TNSA sheath. However, time-of-flight dispersion in the proton beam (see Table 1) dictates that the separation must be minimal to keep heating as isochoric as possible. Also, the angular divergence of the proton beam causes the heating to be greater for smaller foil separations (see Section 2.4.3). Both effects motivate <200μm separations, with <100μm desirable. Previous experiments have generally had source-to-sample separations in the 150-400μm range. Separations <100μm should be possible but require higher accuracy sample foil placement, meaning that more costly engineered targets are needed.

On a related note, the probed sample time frame cannot exceed the hydrodynamics time for the source foil material to reach the sample. Reports have shown time scales of 400ps for 160 μm separation, i.e. 400km/s, and 500ps for 300μm separation, i.e. 600km/s. This indicates that, if the WDM conditions are desired for a 100μm foil separation, one can only explore at least up to 100-200ps before the data is corrupted by this effect.

Table 1: Time of flight dispersion for various proton energies.

Proton Energy (MeV)	v/c	Transit Time for 100mm (ps)	Transit Time for 300mm (ps)
0.5	0.033	10.2	30.7
1	0.046	7.2	21.7
5	0.103	3.2	9.7
10	0.145	2.3	6.9
20	0.203	1.6	4.9
30	0.247	1.3	4.1

2.4.3 Proton Heating Estimates

Proton stopping ability in materials is well known. Using published proton stopping powers for aluminum [15](a common sample material in these experiments) in conjunction with proton source data, one can estimate the amount of heating observed in existing experiments and expected in a potential experiment on the 100TW module of Sandia's Z-Petawatt laser system. The methodology is as follows:

- Get a fit to data of the dN/dE vs proton energy E. Use a fit form $dN/dE=(N_0/(2\cdot E\cdot k_BT)^{1/2})\cdot\exp[-(2\cdot E/k_BT)^{1/2}]$ [16] (see Figure 3).
- Determine the proton source size vs. E. To do this, take data (such as from[14]) and use a linear fit for one heating estimate or use an inverted Gaussian fit [17] for a lower estimate (due to infinite size estimate approaching E=0 MeV)
- Determine the angular divergence (half angle) vs. E. To do this, take data (such as from [18]) and fit with parabolic form[19].For a reassurance, this data gives close to the 20° half angle at 14MeV measured on the Sandia 100TW laser[16].

- Determine the resulting proton beam size at the sample vs. E by accounting for the angular divergence.
- Convert to a sample proton area vs. E
- Take product of the proton spectra data (dN/dE vs. E) and the stopping power (in terms of MeV/cm/proton vs. E (see (Figure 4) and divide by the sample proton area vs. E.

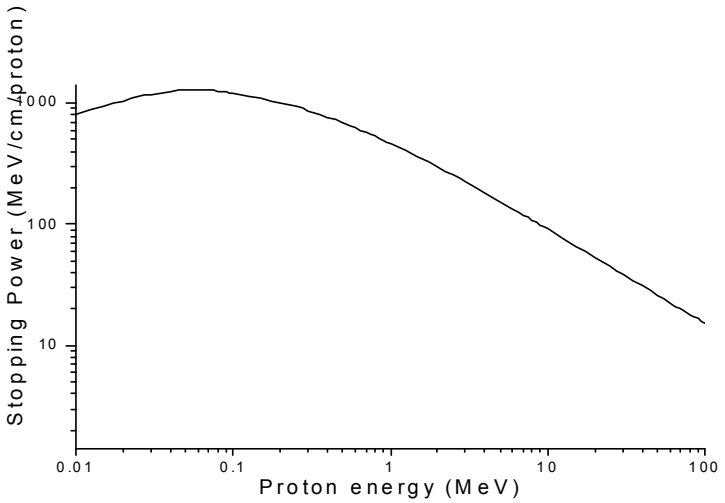

Figure 4. Aluminium stopping power vs. energy

- Integration of this plot yields the net deposited energy in units of MeV/cm^3.
- Division of this integrated number by the number density (6.02×10^{22} atoms/cm^3 for Al) gives the heating/deposited energy in eV/atom

As a caveat, the approach assumes an infinitely thick sample foil, allowing for full absorption of the protons. In fact, the highest energy protons may range through the sample foil due to their reduced stopping power (see Fig. 4). However, there are far fewer of these protons with enough energy to get through the sample foil (see Fig. 3), meaning that most of the protons (which are of lower energy) will in fact go into heating of a reasonable multi-micron thick foil.

The outlined method leads to reasonable albeit perhaps conservative estimates. The benchmark case was Patel *et al* [14], which showed 4±1 eV heating at 250μm foil spacing for a 10J laser. Using the above estimate methodology, the linear proton source fit gives 2.9 eV/atom and the Gaussian source fit gives 1.8 eV/atom. Using the actual Sandia 100TW proton spectra (Fig. 3) and shifting the proton source size vs. E data to match up with higher cut-off proton energy, one gets the estimates in Table 2.

Table 2: Individual atom temperature vs. source-sample separation

Source-to-Sample Foil Separation (μm)	Heating Estimate from Linear Fit to Proton Divergence Data (eV/atom)	Heating Estimate from Gaussian Fit to Proton Divergence Data (eV/atom)
50	26.5	13.0
100	21.0	10.8
250	11.9	6.9
400	7.6	4.9

For comparisons, note that the spacing of 250μm is the same as that in [14] but the heating estimate in Table 2 is higher than the reported 4eV in accordance with the estimate laser energy being higher (40J instead of 10J). Similarly, the spacing of 400μm is the same as that in [12] but the heating estimate in Table 2 is lower than the reported peak heating of 20eV in accordance with the estimate laser energy being lower (40J instead of 100J). Based upon the comparisons and the benchmark, we have confidence that the model is reasonable and probably conservative in its estimates. As such, we can have confidence that the Sandia 100TW laser system should be able to reach WDM states with temperatures >20eV.

3. VARIOUS DIAGNOSTICS TECHNIQUES FOR PROTON HEATING

3.1. Proton Source Characteristic Measurements

Proton beam characterization is very important in order to know the energy loading of the sample target. The proton source can be well characterized using a stack of calibrated radiochromic film (RCF)[20], either in situ[10] or ex situ[14] to the isochoric heating experiment. For better resolution, a Thompson parabola/proton spectrometer[12] can measure various proton energies without the discretization seen in RCF and a diode time-of-flight technique can be used to resolve the maximum (cut-off) proton energy.

3.2. Sample Temperature Diagnostics

Sample temperatures have been measured using streaked optical pyrometry (SOP)[10, 12, 14, 21, 22] in which the optical blackbody emission from the rear foil surface is imaged onto a streak camera (ps resolution or better). This measurement shows the temporal decay of the heated sample on one axis and the 1-D spatial extent of the heated sample on the other axis. Narrowband filters centered at 570nm[14] and 470nm[12] have been used to avoid excessive optical transition radiation (OTR) in 500-550nm range[7]. Attempts have been made to calibrate the transmissive optics and the streak camera in order to measure the absolute target emission at a single wavelength. So far, the accuracy is on the order of ±25% [14], with better results possible (±15% [12]and ±8 [21]).

In general, the measurement may be accurate but the assumption of volumetric heating may not be valid. If the front surface of the sample is heated inhomogeneously[10], the rear surface measurement may not be valid for the entire volume. This issue brings up questions of validity in reports that show the heating reduced for thicker sample foils [23].

In non-streaked pyrometry, a two-color method can determine temperatures directly via the ratio of the collected intensities while assuming a blackbody radiation profile, avoiding some of the calibration issue. Such non-streaked two-color pyrometers usually show better accuracy than their one-color counterparts [24]. As such, a two-color SOP is desired. Ideally, such a device will image two spectrally and spatially separate images of the sample foil onto the streak camera, allowing for two different spatially resolved measurements. With the anticipated improvement in accuracy, a two-color SOP may have ±5% error.

As an alternative diagnostic, XUV imaging at 68 and 256 eV[25] gives time-integrated 2D spatial data but calibration/absolute temperature measurement may be difficult. The information is complimentary to the SOP data and could help with alignments.

3.3. Sample Pressure/Velocity Diagnostics

Pressures/expansion velocities have been measured several ways, generally using an optical probe at the 2^{nd} and 3^{rd} harmonic ($2\omega/3\omega$) of the main pulse[3, 10-12, 14]. This avoids scatter

from the main pulse fundamental (1ω) and also improves the transmission through the plasma. The proximity of source and sample allow 2 basic configurations:

3.3.1. Side-on optical Probe

Because the proton source target and the sample are so close, the laser probe beam will always skim the rear surface of the target and the front surface of the sample. This beam can directly provide shadowgraph over the probe laser pulse duration. Interferometric data can be acquired using lateral or radial shear interferometry. Furthermore, Dark Field/Schlieren[26] and Faraday rotation techniques could be employed. This approach is essential in examining front surface heating of the sample and determining hydrodynamics time frames for the source foil to reach the sample foil.

3.3.2. Rear-surface Reflection Probe

A rear surface reflection probe can show reflectivity changes in the sample as well as the temporal shift of the reflecting surface. This technique often uses spectral interferometry (requiring an unchirped probe) or chirped pulse interferometry (CPI) (requiring a chirped probe). The basic concept here is to create an interferometer where one arm serves as reference and one probes the sample. Upon recombination of the beams, a spectrometer stretches the beam temporally such that the reference and probe overlap in time, allowing the two pulses to show spectral interference. Using unchirped pulses requires a variety of delays to be employed in a pump-probe scenario, with the main assumption being that the experimental conditions are identical. Since in fact conditions are rarely identical but may at best be similar, a single-shot method can be created if the probe and reference are partially stretched (chirped) prior to entering the experimental setup. The diagnostic provides spatial resolution in one axis and spectral (which is also temporal) resolution in the other axis. As such, the CPI provides a similar spatial-temporal plot to streak cameras (and hence VISAR) but the synchronization of the CPI probe beam avoids potential trigger jitter difficulties that might occur with a high-speed streak camera.

Resolution is temporally limited by the spectral resolution of the spectrometer in the setup and the chirp (which is about 2ps for 0.1nm spectrometer resolution and 50nm/ns chirp for 5nm bandwidth stretched to 100ps probe duration) and spatially to the fringe resolution (usually a best case of about 1/50 of the wavelength or 0.02μm). This allows experimental resolution of roughly 0.01μm/ps or 10km/s, a value commensurate with CPI experimental data [12].

4. PROPOSED EXPERIMENTAL SETUP

4.1. General constraints to optimize isochoric heating experiment

- Employ proton heating due to high efficiency of process
- Optimize the proton source to optimize the heating. Optimize laser energy, pulsewidth, intensity, contrast, polarization, angle of incidence. Furthermore, optimize source material, contaminant layer (custom layers/target cleaning), and source target size. Explore proton focusing/shaping methods such as hemispherical source targets and spatially shaped prepulses.
- Mitigate collateral heating effects from x-rays, co-moving electrons, or laser heating. Thicker source foils will not burn through in time to expose the sample target to any residual laser light. Poor conversion efficiency and the isotropic/non-directionality of the x-rays make their contribution irrelevant.
- Tailor the proton spectra to achieve heat uniformly throughout the sample (if possible).
- Heat the sample in a timeframe less than the expansion time (to be isochoric). This means that the distances from the source to the sample must be as small as possible to minimize heating pulse spread associated with proton energy dispersion. On the other hand, one needs to maintain enough distance so as not to affect TNSA.
- Heat a thick enough sample such that the expansion time is longer than the electron-ion equilibration time
- Model data using EOS tables and a radiative hydrodynamics code.

4.2. Required Laser Parameters

- The wavelength is fixed at 1054nm. This is advantageous for hot electron/proton creation via $I\lambda^2$ heating.
- Relativistic regime is required for proton generation: $I > 10^{18}$ W/cm^2.
- For maximum sample heating and to access a newer regime of WDM temperatures, the laser energy has to exceed: E > 50J.
- For isochoric heating of targets 1-10μm thick, the pulsewidth has to be <1ps (preferrable <500fs).
- The resulting spot size based on the previous parameters is <50μm diameter.
- For probe beam alignments at a 300μm target field of view, the pointing stability needs to be < ±150μm .
- A contrast of $<10^8$ is required for better proton production[27, 28]. Generally, the high energy proton cut-off increases with increasing intensity[26] and decreasing target thickness, with similar trending for the overall proton yield. Given that thinner targets also require higher contrast to avoid pre-pulse burn-through, the contrast should be as high as possible. Note that pre-pulses can disturb the sheath development in TNSA, explaining why the high energy cutoff in the presence of unspecified pre-pulses degrades from the ideal infinite contrast limit. A properly *controlled* pre-pulse may be of sufficiently low energy so as not to spoil the TNSA process while creating an appropriate scale-length plasma for optimal laser absorption.

4.3. Available Drive Laser: Z-Petawatt

The Z-Petawatt laser (Figure 5) uses chirped pulse amplification to achieve high intensities. In this technique, the initial short pulse gets temporally stretched in order to amplify it safely at the reduced power. After amplification, the beam is re-compressed to achieve maximum intensities

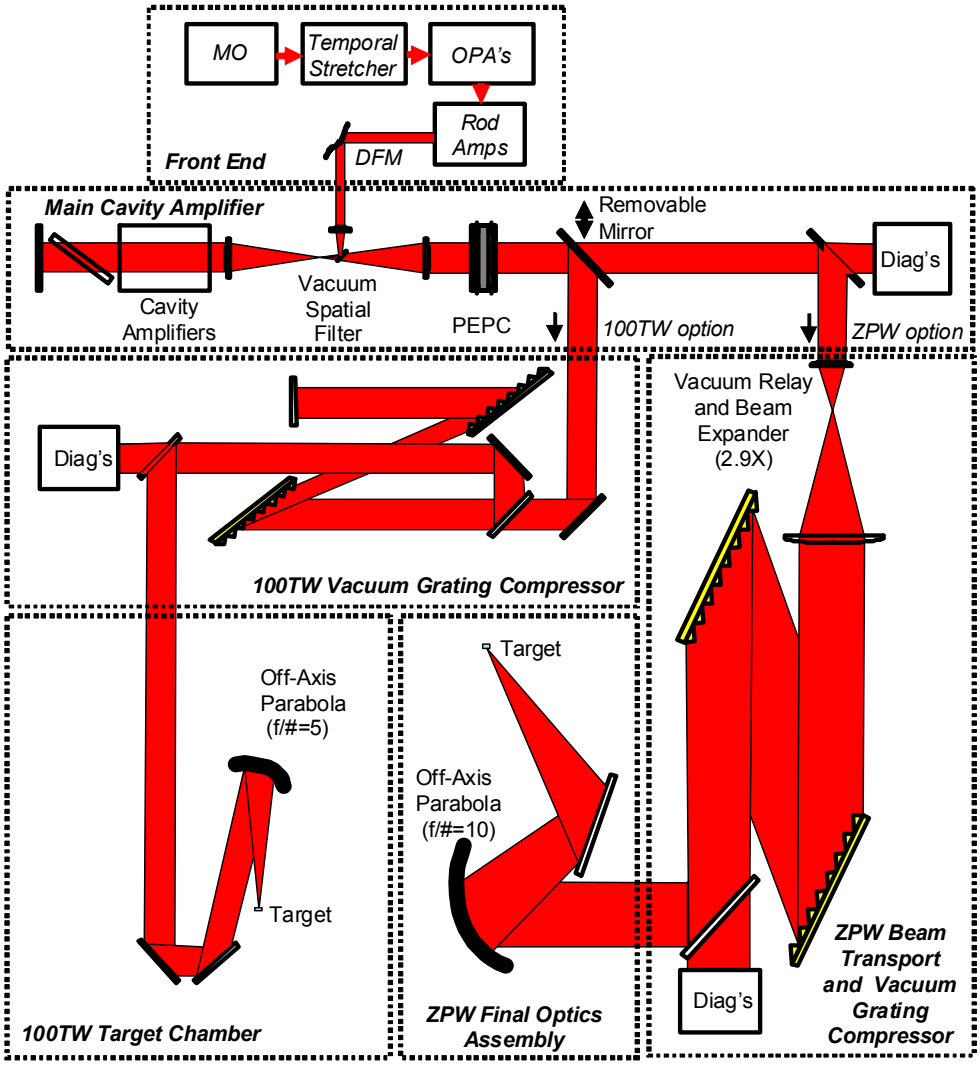

Figure 5. Schematic of the Z-Petawatt laser system

The Z-Petawatt system operation is determined by the size of the temporal compressor gratings chosen:

- 100TW option at 50 J/500 fs: Uses smaller gratings but has a developed Target Area with short f/# parabola. This system can achieve relativistic intensities up to 10^{19} W/cm^2.
- ZPW option at 500 J/500 fs: Larger gratings, but a Target Area is pending. This system can achieve relativistic intensities up to 10^{20} W/cm^2.

The lack of a Target Area and probe beams on Z-Petawatt means that only the 100TW system is available for isochoric heating experiments at the moment.

4.4. Available Target Area Infrastructure

4.4.1. 100 TW target interaction chamber

The stainless steel vessel has a diameter of 1.5m with removable domes sides. It can reach a vacuum pressure of $<10^{-6}$ Torr within 1 hour when pumping down from atmospheric pressure. An f=62.5cm off-axis parabola (f/#=4.2) can focus the laser beam to 7μm FWHM.

4.4.2. Lasers

The drive laser has a center wavelength of 1054 nm with an energy of 50 J and a pulsewidth < 1 ps resulting in an intensity of 10^{19} W/cm^2. Pointing stability is < 50 μm. An optical probe beam is taken via a pick-off of the front-end output before amplifiers are seeded. This beam is available with a wavelength of 1054/527 nm with energy of 30/10 mJ and a pulsewidth of < 500 fs. Probe beam time delays can be varied from ps to multiple ns.

4.4.3. Target Chamber Diagnostics

- K-α imager (8keV)
- X-ray pin-hole cameras
- Multiple X-ray and optical streak cameras,
- 200 fs resolution@1:40 dynamic range, 5 ps@1:1000
- Various X-ray and optical spectrometers
- Single photon counting CCD's
- 12 GHz digital scopes
- Thompson parabola
- HV supplies up to 20 kV
- IP and CR39 detectors
- EMI shielded instrumentation cabinets up to 120 dB

4.5. Proposed Diagnostics for an Experimental Run

4.5.1. Streaked Optical Pyrometry (SOP)

This technique will yield a time resolved temperature measurement by imaging the blackbody radiation from the rear side of the sample onto a streak camera. It requires an accurately calibrated streak camera with a time resolution of < 5ps. The available Hamamatsu FESCA with

a resolution of < 1ps fulfills that requirement but the photocathode is only sensitive at longer wavelengths. A slightly slower Hamamatsu visible streak camera is also available. A 2-color SOP for improved accuracy would be desirable for the future.

4.5.2. Proton Diagnostics

A Thompson parabola/proton spectrometer as well as CR39 and RCF will be used to determine the proton energy distribution from the source target. All these diagnostic tools are available in house.

4.5.3. Chirped Pulse Interferometry (CPI)

CPI will allow measuring the expansion velocity of the sample's rear surface during the first 10's of ps. This requires a bright probe beam that can be partially recompressed independent from the main pulse. Stabilization of the beam pointing may be required based on previous experience.

4.5.4. Side-on Interferometry/Shadowgraphy

This is not a single-shot diagnostic like CPI but it can also measure the sample's expansion velocity via a series of time delayed snap shots. With this technique one should be able to characterize laser pre-pulse effects as well as plasma propagation from the source target foil to the sample foil. Furthermore, nonuniformities in heating between the front and rear surface of the sample foil should be apparent. We propose doing this with a small spatial pick-off of the main beam within the target vessel. An adjustable delay and relay-image telescope with optional spatial filtering are likely.

The interplay of these various diagnostics is represented in Figure 6.

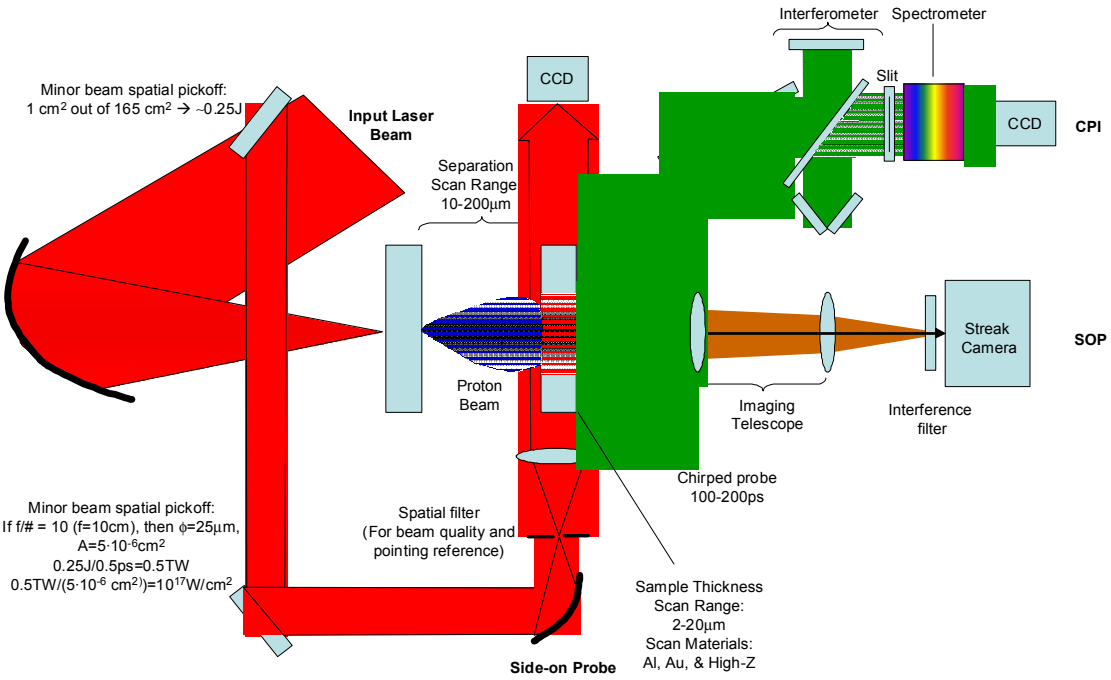

Figure 6. Proposed experimental setup

5. DEVELOPMENTAL TIMEFRAME

Figure 7 shows the proposed time frame for a 3 year experimental effort focusing on such WDM/isochoric heating methods. Interspersed with various experimental runs on the laser will be different diagnostic and target development efforts. When the basic diagnostic components are active, experimental campaigns will transition to higher Z materials and look at hemispherical targets as well as reduced source-to-sample foil separations, all with the intent of improving the amount of heating. In conjunction with this will be a variety of diagnostic improvements including the two-color SOP and multi-wavelength XUV imaging. By the end of the period, one would hope that diagnostic improvements like this will allow accurate exploration of the proposed heating regime.

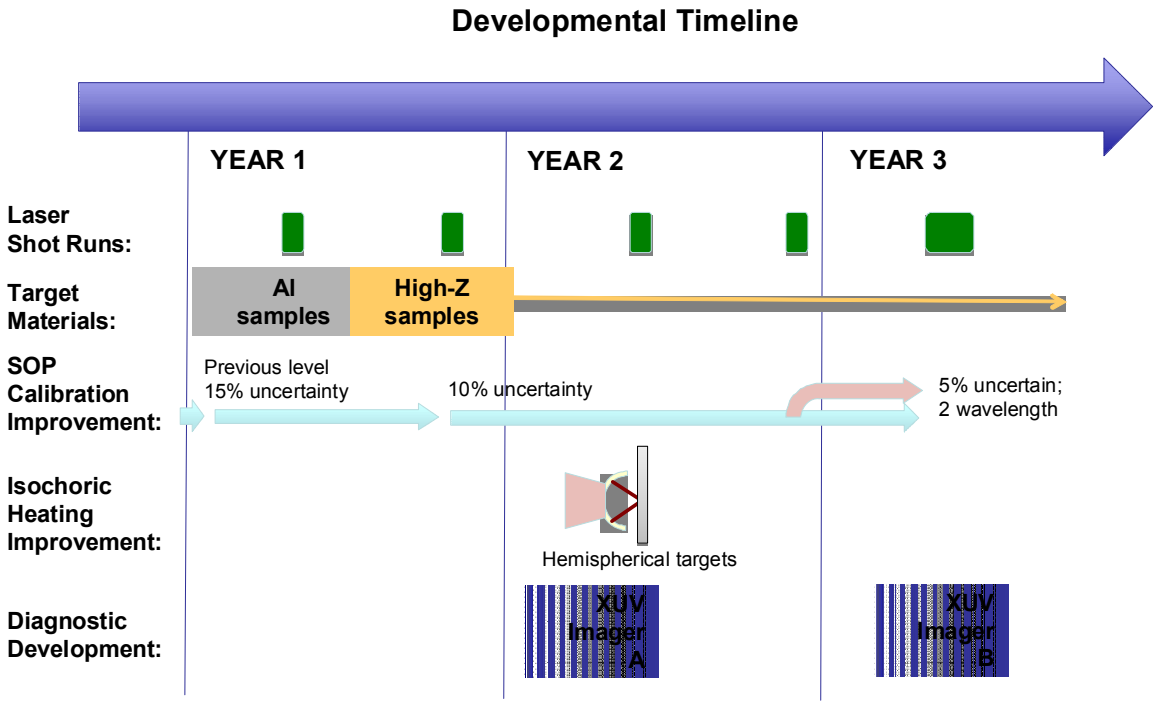

Figure 7. Proposed timeframe for the study of WDM in the laboratory.

REFERENCES

1. Hansen, S.B., et al., *Temperature determination using K alpha spectra from M-shell Ti ions.* PHYSICAL REVIEW E, 2005. **72**(3, 2).
2. Saemann, A., et al., *Isochoric heating of solid aluminum by ultrashort laser pulses focused on a tamped target.* Physical Review Letters, 1999. **82**(24): p. 4843-4846.
3. Widmann, K., et al., *Interferometric investigation of femtosecond laser-heated expanded states.* Physics of Plasmas, 2001. **8**(9): p. 3869-3872.
4. Audebert, P., et al., *Heating of thin foils with a relativistic-intensity short-pulse laser.* Physical Review Letters, 2002. **89**(26): p. 265001-1-265001-265001-4.
5. Evans, R.G., et al., *Rapid heating of solid density material by a petawatt laser.* Applied Physics Letters, 2005. **86**(19): p. 191505-1-191505-191505-3.
6. Key, M.H., et al., *Study of electron and proton isochoric heating for fast ignition.* Journal de Physique IV (Proceedings), 2006. **133**: p. 371-8.
7. Nakatsutsumi, M., et al., *Heating of solid target in electron refluxing dominated regime with ultra-intense laser.* Journal of Physics: Conference Series, 2008. **112**(2): p. 022063 (4 pp.)-022063 (4 pp.).
8. Dyer, G., et al., *Isochoric heating of solid aluminium with picosecond X-ray pulses.* Journal of Modern Optics, 2003. **50**(15-17): p. 2495-2505.
9. Wilks, S.C., et al., *Energetic proton generation in ultra-intense laser-solid interactions.* Physics of Plasmas, 2001. **8**(2): p. 542-549.
10. Brambrink, E., et al., *Direct evidence of strongly inhomogeneous energy deposition in target heating with laser-produced ion beams.* Physical Review E (Statistical, Nonlinear, and Soft Matter Physics), 2007. **75**(6): p. 65401/1-65401/4.
11. Dyer, G., et al. *Single-shot time resolved expansion and emission measurements of proton-heated warm dense matter*. 2007.
12. Dyer, G.M., et al., *Equation-of-state measurement of dense plasmas heated with fast protons.* PHYSICAL REVIEW LETTERS, 2008. **101**(1).
13. Malka, G., et al., *Fast electron transport and induced heating in solid targets from rear-side interferometry imaging.* Physical Review E (Statistical, Nonlinear, and Soft Matter Physics), 2008. **77**(2): p. 026408-1-026408-026408-8.
14. Patel, P.K., et al., *Isochoric heating of solid-density matter with an ultrafast proton beam.* Physical Review Letters, 2003. **91**(12): p. 125004/1-125004/4.
15. NIST. *PSTAR-proton stopping powers*. [cited; Available from: http://physics.nist.gov/PhysRefData/Star/Text/PSTAR.html.
16. Schollmeier, M., et al., *Controlled transport and focusing of laser-accelerated protons with miniature magnetic devices.* PHYSICAL REVIEW LETTERS, 2008. **101**(5).
17. Schollmeier, M., et al., *Laser beam-profile impression and target thickness impact on laser-accelerated protons.* Physics of Plasmas, 2008. **15**(5): p. 053101-1-12.
18. Snavely, R.A., et al., *Intense high-energy proton beams from petawatt-laser irradiation of solids.* Physical Review Letters, 2000. **85**(14): p. 2945-8.
19. Schollmeier, M., et al., *Laser ion acceleration with micro-grooved targets.* Nuclear Instruments & Methods in Physics Research, Section A (Accelerators, Spectrometers, Detectors and Associated Equipment), 2007. **577**(1-2): p. 186-90.

20. Eagleton, R.T., et al., *Target diagnostics for commissioning the AWE HELEN Laser Facility 100 TW chirped pulse amplification beam.* REVIEW OF SCIENTIFIC INSTRUMENTS, 2006. **77**(10).
21. Miller, J.E., et al., *Streaked optical pyrometer system for laser-driven shock-wave experiments on OMEGA.* REVIEW OF SCIENTIFIC INSTRUMENTS, 2007. **78**(3).
22. Shigemori, K., et al., *Shock pyrometry of laser-irradiated foils below 1eV.* JAPANESE JOURNAL OF APPLIED PHYSICS PART 1-REGULAR PAPERS BRIEF COMMUNICATIONS & REVIEW PAPERS, 2006. **45**(5A): p. 4224-4226.
23. Antici, P., et al. *Application of laser-accelerated high-energy protons for isochoric heating of matter*. in *32nd EPS conference on plasma physics*. 2005,Tarragona.
24. Muller, B. and U. Renz, *Development of a fast fiber-optic two-color pyrometer for the temperature measurement of surfaces with varying emissivities.* REVIEW OF SCIENTIFIC INSTRUMENTS, 2001. **72**(8): p. 3366-3374.
25. Patel, P.K., et al., *Integrated laser-target interaction experiments on the RAL petawatt laser.* PLASMA PHYSICS AND CONTROLLED FUSION, 2005. **47**(12B, SI): p. B833-B840.
26. Beg, F.N., et al., *A study of picosecond laser-solid interactions up to 10(19) W cm(-2).* PHYSICS OF PLASMAS, 1997. **4**(2): p. 447-457.
27. Kaluza, M., et al., *Influence of the laser prepulse on proton acceleration in thin-foil experiments.* Physical Review Letters, 2004. **93**(4): p. 045003/1-4.
28. Mackinnon, A.J., et al., *Effect of plasma scale length on multi-MeV proton production by intense laser pulses.* Physical Review Letters, 2001. **86**(9): p. 1769-72.

Distribution

1	MS1193	Briggs Atherton	Org. 1672	
1	MS1191	John Porter	Org. 1670	
1	MS1193	Patrick Rambo	Org. 1672	
1	MS1193	Jens Schwarz	Org. 1672	
2	MS0899	Technical Library	Org. 9536	(electronic copy)
1	MS0123	D. Chavez, LDRD Office	Org. 1011	


Sandia National Laboratories